Bioconjugate Chemistry

Article

Cite This: Bioconjugate Chem. 2018, 29, 410−419

pubs.acs.org/bc

Positron Emission Tomography Imaging of Prostate Cancer with Ga-68-Labeled Gastrin-Releasing Peptide Receptor Agonist BBN_{7-14} and Antagonist RM26

Siyuan Cheng,[†,‡] Lixin Lang,[‡] Zhantong Wang,[‡] Orit Jacobson,[‡] Bryant Yung,[‡] Guizhi Zhu,[‡] Dongyu Gu,[‡] Ying Ma,[‡] Xiaohua Zhu,[*,†] Gang Niu,[*,‡] and Xiaoyuan Chen[*,‡]

[†]Department of Nuclear Medicine and PET, Tongji Hospital, Tongji Medical College, Huazhong University of Science and Technology, Wuhan 430000, PR China

[‡]Laboratory of Molecular Imaging and Nanomedicine, National Institute of Biomedical Imaging and Bioengineering (NIBIB), National Institutes of Health (NIH), Bethesda, Maryland 20892, United States

ABSTRACT: Radiolabeled bombesin (BBN) analogs have long been used for developing gastrin-releasing peptide receptor (GRPR) targeted imaging probes, and tracers with excellent in vivo performance including high tumor uptake, high contrast, and favorable pharmacokinetics are highly desired. In this study, we compared the ^{68}Ga-labeled GRPR agonist (Gln−Trp−Ala−Val−Gly−His−Leu−Met−NH_2, BBN_{7-14}) and antagonist (D-Phe−Gln−Trp−Ala−Val−Gly−His−Sta−Leu−NH_2, RM26) for the positron emission tomography (PET) imaging of prostate cancer. The in vitro stabilities, receptor binding, cell uptake, internalization, and efflux properties of the probes ^{68}Ga−1,4,7-triazacyclononane-1,4,7-triacetic acid (NOTA)−Aca−BBN_{7-14} and ^{68}Ga−NOTA−poly(ethylene glycol)$_3$ (PEG_3)−RM26 were studied in PC-3 cells, and the in vivo GRPR targeting abilities and kinetics were investigated using PC-3 tumor xenografted mice. BBN_{7-14}, PEG_3-RM26, NOTA−Aca−BBN_{7-14}, and NOTA−PEG_3−RM26 showed similar binding affinity to GRPR. In PC-3 tumor-bearing mice, the tumor uptake of ^{68}Ga−NOTA−PEG_3−RM26 remained at around 3.00 percentage of injected dose per gram of tissue within 1 h after injection, in contrast with ^{68}Ga−NOTA−Aca−BBN_{7-14}, which demonstrated rapid elimination and high background signal. Additionally, the majority of the ^{68}Ga−NOTA−PEG_3−RM26 remained intact in mouse serum at 5 min after injection, while almost all of the ^{68}Ga−NOTA−Aca−BBN_{7-14} was degraded under the same conditions, demonstrating more-favorable in vivo pharmacokinetic properties and metabolic stabilities of the antagonist probe relative to its agonist counterpart. Overall, the antagonistic GRPR targeted probe ^{68}Ga−NOTA−PEG_3−RM26 is a more-promising candidate than the agonist ^{68}Ga−NOTA−Aca−BBN_{7-14} for the PET imaging of prostate cancer patients.

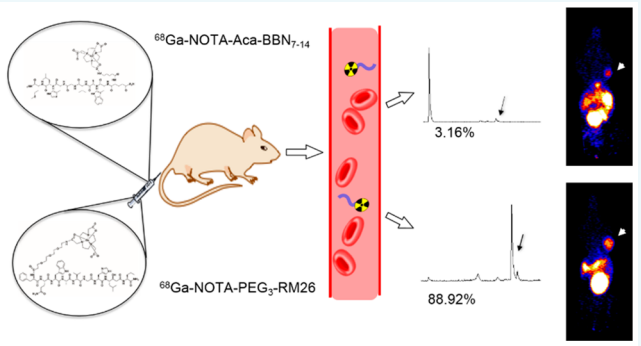

INTRODUCTION

Prostate cancer (PCa) accounts for almost 20% of the newly diagnosed cancers among men in the United States in 2017 and remains the third-leading cause of cancer related male death.[1] A typical diagnosis of PCa relies on the histopathological examination of suspected prostate biopsy tissues or specimens from benign prostatic enlargement surgeries or transurethral resection of the prostate following the detection of elevated prostate-specific antigen (PSA) levels, abnormal digital rectal examination (DRE), bone scanning, or a combination of all three. X-ray computed tomography and magnetic resonance imaging (MRI) are currently the major imaging techniques for further identification of PCa.[2] However, the capacity of conventional diagnostic techniques for primary lesion detection, staging, or relapse monitoring of PCa is limited.[3] For example, the PSA test can be interfered by noncancerous factors such as prostate enlargement, old age, and prostatitis, and low levels of PSA do not necessarily rule out the incidence of PCa.[4] The sensitivity and specificity of either ultrasound or MRI is also limited by abnormal signals confounded by prostatitis or benign prostatic hyperplasia (BPH).[5,6] The notable multiparametric MRI (MP-MRI) remains imperfect as well, with a pooled sensitivity of up to 89% and a specificity of up to 73%.[7]

Interest in applying molecular imaging to positron emission tomography (PET) has grown, and a plethora of radiotracers have been developed and investigated actively for PCa. The classical 2-deoxy-2-^{18}F-fluoro-D-glucose (^{18}F-FDG) has been used for evaluating late-stage or recurrent PCa but is not particularly avid.[8,9] Other promising agents targeting metabo-

Received: November 22, 2017
Revised: December 14, 2017
Published: December 18, 2017

DOI: 10.1021/acs.bioconjchem.7b00726
Bioconjugate Chem. 2018, 29, 410−419

lites such as fatty acids and amino acids (e.g., ^{11}C- and ^{18}F-choline, ^{11}C-acetate, and ^{18}F-FACBC) have been further introduced[3,10] as well as agents targeting specific PCa antigens such as prostate-specific membrane antigen (PSMA).[11,12] These tracers are proven beneficial for recurrent PC diagnosis and staging. The PSMA targeted tracers have also been applied specially for predicting the optimal timing of PSMA-based therapies.[13] However, almost all these tracers show limited diagnostic accuracy for primary lesions,[3,10,14] and few of those tracers have been sufficiently investigated and clinically validated to date.

The gastrin-releasing peptide receptor (GRPR) is a G protein-coupled receptor expressed in various organs of mammals, especially in the gastrointestinal tract and the pancreas. Upon binding with the ligand gastrin-releasing peptide (GRP), GRPR can be activated and elicit certain exocrine or endocrine secretions to regulate multiple physiological processes.[15] Notably, GRPR over-expression is presented in several types of tumors such as prostate, urinary tract, gastrointestinal stromal, breast, and lung and is related to proliferation and growth of these malignancies.[16,17] Especially, GRPR is almost 100% expressed in clinical PCa samples investigated by PCR, immunohistochemistry, or radionuclide binding assays,[16] which makes GRPR an attractive target for PCa imaging and therapy.

As an amphibian homologue of GRP, bombesin (BBN) was found to bind to GRPR with a high affinity. For decades, the BBN motifs have been used extensively in radioactive imaging or in radionuclide therapy for GRPR-over-expressing cancers.[18,19] For example, the GRPR agonist BBN_{7-14}, a truncated form of BBN with the sequence of Gln−Trp−Ala−Val−Gly−His−Leu−Met−NH_2, has been studied as PET or single photon emission computed tomography (SPECT) tracers in both preclinical and clinical research.[20−23] In the meantime, numerous clinical trials have been performed using antagonistic GRPR targeting PET radiopharmaceuticals including ^{68}Ga−RM2,[24,25] ^{68}Ga−SB3,[26] ^{68}Ga−BAY86−7458,[27] and ^{64}Cu−CB−TE2A−AR06.[28] Recently, a nine-amino-acid analog of non-apeptide BBN_{6-14}, D-Phe−Gln−Trp−Ala−Val−Gly−His−Sta−Leu−NH_2 (RM26) has been developed as an antagonist against GRPR and has been applied actively in preclinical studies.[29−32] Based on these observations, both BBN_{7-14} and RM26 are considered high-quality candidates for further clinical translation.

Despite the outstanding tumor targeting potential, BBN related research is accompanied by a debate on the superiority of GRPR antagonist- versus agonist-based tracers.[33−36] It is generally claimed that even though antagonists are not internalized, radiolabeled antagonists may depict clearer images and pharmacokinetic profiles than agonists. More data are expected to emerge for direct comparison of specific radiolabeled agonist and antagonist tracers to address this controversy, especially among tracers that are promising for clinical translation.

Herein, we establish the distinction of GRPR targeted agonist and antagonist with similar sequences by applying ^{68}Ga-labeled BBN_{7-14} and RM26 for side-by-side comparative studies, including in vitro receptor binding, cell uptake, internalization, and efflux studies on PC-3 cells and in vivo microPET imaging study of PC-3 tumor bearing mice. The in vitro and in vivo stabilities of both radio conjugates were presented and compared as well.

RESULTS

Synthesis and Radiolabeling. With excess amounts of 1,4,7-triazacyclononane-1,4,7-triacetic acid (NOTA)−*N*-hydroxysuccinimide (NHS), the NOTA−Aca−BBN_{7-14} and NOTA−poly(ethylene glycol)$_3$ (PEG_3)−RM26 conjugate were produced in >95% yield. A m/z of 1338 for [M + H^+] was identified for NOTA−Aca−BBN_{7-14} using matrix-assisted laser desorption ionization−time-of-flight mass spectrometry (MALDI−TOF MS). NOTA−PEG_3−RM26 was synthesized and characterized by the same method (m/z = 1601 for [M + H^+]). Both conjugates were labeled with ^{68}Ga within 20 min, with specific activities of 21.6−40.01 and 26.7−53.33 MBq/nmol, respectively, for ^{68}Ga−NOTA−Aca−BBN_{7-14} and ^{68}Ga−NOTA−PEG_3−RM26, and for both, radiochemical yield was >90−95% and radiochemical purity was >98%. The chemical structures of ^{68}Ga−NOTA−Aca−BBN_{7-14} and ^{68}Ga−NOTA−PEG_3−RM26 were presented in Figure 1.

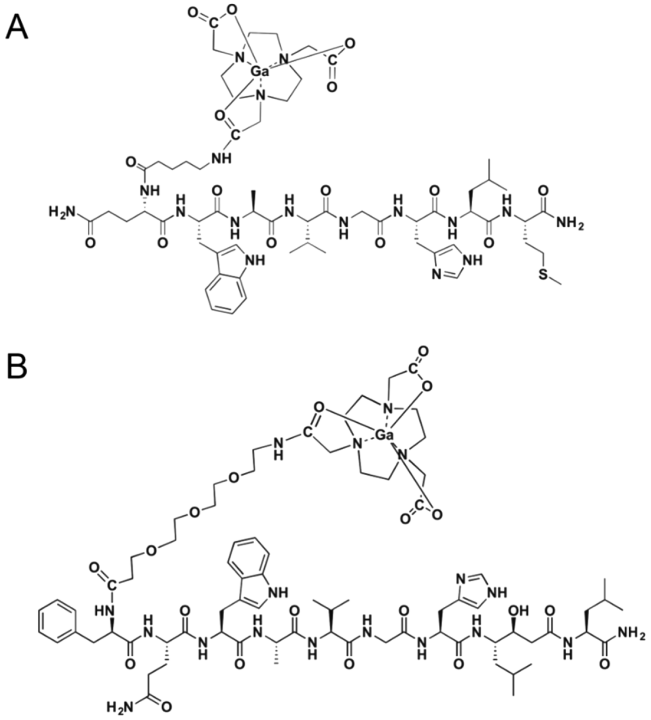

Figure 1. Schematic structures of (A) GRPR agonist ^{68}Ga−NOTA−Aca−BBN_{7-14} and (B) antagonist ^{68}Ga−NOTA−PEG_3−RM26.

In Vitro Stability. In vitro stabilities of ^{68}Ga−NOTA−Aca−BBN_{7-14} and ^{68}Ga−NOTA−PEG_3−RM26 in saline and nonheat-inactivated fetal bovine serum (FBS) (Gibco) were determined according to peak integration of analytical high-performance liquid chromatography (HPLC). At 0 min of the incubation, the radiochemical purities of ^{68}Ga−NOTA−Aca−BBN_{7-14} and ^{68}Ga−NOTA−PEG_3−RM26 were all >95% in both saline and FBS (Figure 2). After 2 h of incubation, the parent compound of ^{68}Ga−NOTA−Aca−BBN_{7-14} in saline dropped to 88.42% along with a more-hydrophilic peak of 11.58%, while this metabolism for ^{68}Ga−NOTA−Aca−BBN_{7-14} incubated in FBS was not as obvious. Metabolites represented by radio peaks of slightly higher lipophilicity than the parent compounds were observed for both after 2 h incubation in FBS, accompanied by the percentages of the parent compounds dropping to 89.24% and 80.58%,

DOI: 10.1021/acs.bioconjchem.7b00726
Bioconjugate Chem. 2018, 29, 410−419

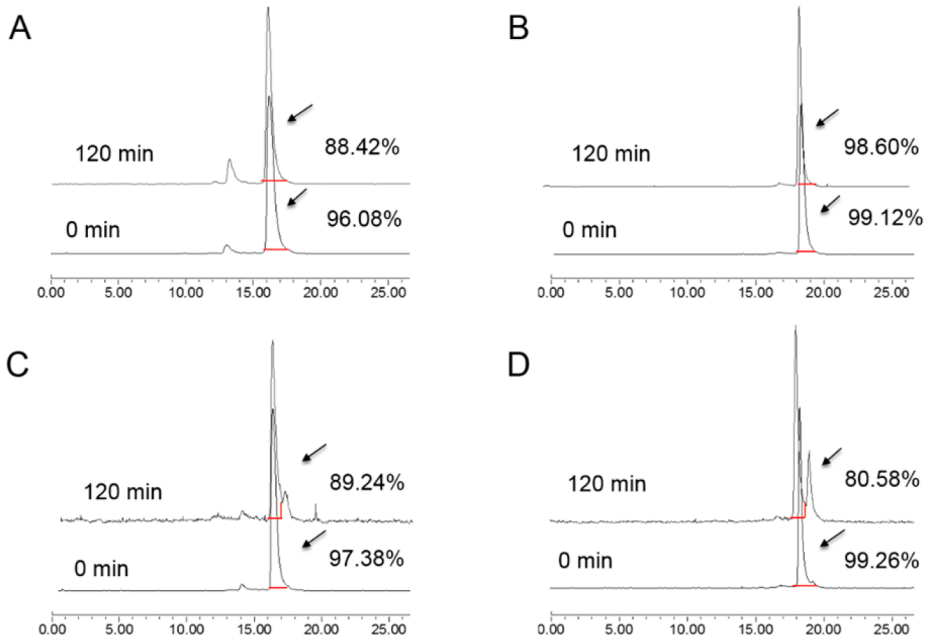

Figure 2. In vitro radioactive stabilities of ^{68}Ga−NOTA−Aca−BBN$_{7-14}$ and ^{68}Ga−NOTA−PEG$_3$−RM26 in saline and fetal bovine serum (FBS) for 0 and 120 min after incubation. (A) In vitro radioactive stabilities of ^{68}Ga−NOTA−Aca−BBN$_{7-14}$ in saline at 0 and 120 min after incubation. (B) In vitro radioactive stabilities of ^{68}Ga−NOTA−PEG$_3$−RM26 in saline at 0 and 120 min after incubation. (C) In vitro radioactive stabilities of ^{68}Ga−NOTA−Aca−BBN$_{7-14}$ in FBS at 0 and 120 min after incubation. (D) In vitro radioactive stabilities of ^{68}Ga−NOTA−PEG$_3$−RM26 in FBS at 0 and 120 min after incubation.

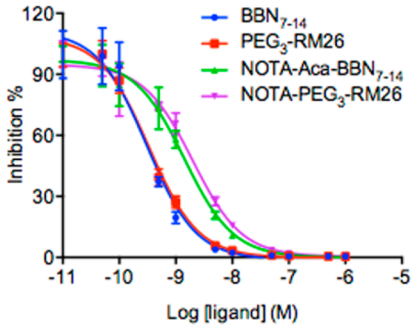

Compound	IC$_{50}$ (nM)
BBN$_{7-14}$	0.32 ± 0.10
PEG$_3$-RM26	0.41 ± 0.13
NOTA-Aca-BBN$_{7-14}$	1.80 ± 0.67
NOTA-PEG$_3$-RM26	2.05 ± 0.50

Figure 3. Inhibition of ^{125}I−[Tyr^4]BBN binding to GRPR on PC-3 cells by BBN$_{7-14}$, PEG$_3$-RM26, NOTA−Aca−BBN$_{7-14}$, and NOTA−PEG$_3$−RM26 (n = 3/group, mean ± SD).

respectively, for ^{68}Ga−NOTA−Aca−BBN$_{7-14}$ and ^{68}Ga−NOTA−PEG$_3$−RM26.

Competitive Binding Assay. The GRPR-binding affinities of BBN$_{7-14}$, PEG$_3$−RM26, NOTA−Aca−BBN$_{7-14}$, and NOTA−PEG$_3$−RM26 were assessed by competitive binding assay using ^{125}I−−Tyr^4]BBN as the radioligand. The results of these assays were shown in Figure 3. The binding of ^{125}I−[Tyr^4]BBN to GRPR was displaced by the cold analogs in a concentration-dependent manner. The half maximal inhibitory concentration (IC$_{50}$) values of BBN$_{7-14}$, PEG$_3$−RM26, NOTA−Aca−BBN$_{7-14}$, and NOTA−PEG$_3$−RM26 were 0.32 ± 0.10, 0. 41 ± 0.13, 1.80 ± 0.67, and 2.05 ± 0.50 nM, respectively. The results indicated that the intermolecular targeting abilities of BBN$_{7-14}$ and PEG$_3$−RM26 for GRPR were comparable. After the NOTA conjugation, the affinities of both compounds decreased to some extent. However, there were no distinct disparities discovered between NOTA−Aca−BBN$_{7-14}$ and NOTA−PEG$_3$−RM26, either.

Cell Uptake, Internalization, and Efflux. A time-dependent cellular-uptake pattern in GRPR positive PC-3 cells was observed for both ^{68}Ga−NOTA−Aca−BBN$_{7-14}$ and ^{68}Ga−NOTA−PEG$_3$−RM26. The uptake of ^{68}Ga−NOTA−Aca−BBN$_{7-14}$ increased rapidly to nearly 27% within 1 h of incubation, and that of ^{68}Ga−NOTA−PEG$_3$−RM26 was slightly lower (Figure 4A). The agonist ^{68}Ga−NOTA−Aca−BBN$_{7-14}$ showed distinctively high internalization, and around 74% of the radioactivity uptake was internalized within 1 h of incubation. In contrast, ^{68}Ga−NOTA−PEG$_3$−RM26 showed very low internalization (<15% of total uptake; Figure 4A). After washing and medium replacement, both of the tracers showed efflux with a similar pattern (Figure 4B). At 60 min, 50% of radioactivity uptake was still retained with the cells.

In Vivo PET Imaging. Representative coronal PET images of PC-3 tumor-bearing mice at different time points are shown in Figure 5. The tumors were clearly visualized with high contrast at all the time points for ^{68}Ga−NOTA−PEG$_3$−RM26 (n = 3) as well as at 15 and 30 min for ^{68}Ga−NOTA−Aca−BBN$_{7-14}$ (n = 4). However, at 60 min post-injection, the tumor became much less visible in the mice administered with ^{68}Ga−NOTA−Aca−BBN$_{7-14}$ (Figure 5A). Meanwhile, both of the

DOI: 10.1021/acs.bioconjchem.7b00726
Bioconjugate Chem. 2018, 29, 410−419

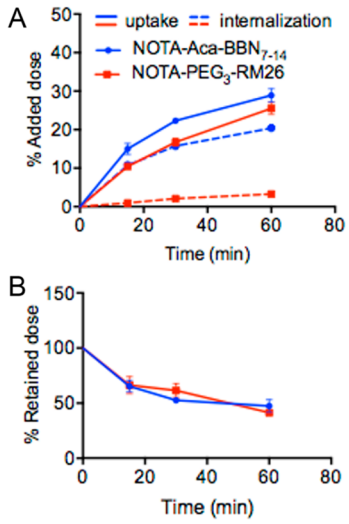

Figure 4. In vitro cell uptake, internalization, and efflux studies of ^{68}Ga−NOTA−Aca−BBN$_{7-14}$ and ^{68}Ga−NOTA−PEG$_3$-RM26 on PC-3 cells. (A) Cell uptake and internalization assay of ^{68}Ga−NOTA−Aca−BBN$_{7-14}$ and ^{68}Ga−NOTA−PEG$_3$−RM26 on PC-3 tumor cells (n = 3, mean ± SD). (B) Cell efflux assay of ^{68}Ga−NOTA−Aca−BBN$_{7-14}$ and ^{68}Ga−NOTA−PEG$_3$−RM26 on PC-3 tumor cells (n = 3, mean ± SD).

tracers showed considerable accumulation and retention in the abdominal regions including pancreas and intestines, although less was observed for ^{68}Ga−NOTA−PEG$_3$−RM26 than for ^{68}Ga−NOTA−Aca−BBN$_{7-14}$. At these early time points, relatively high kidney radioactivity was observed while the radioactivity in the bladder was constantly high for these two probes, suggesting that the tracers were excreted mainly by the renal system.

Activity accumulation in the tumor was quantified by measuring the regions of interest (ROIs) on the coronal images (Figure 5B,C). The mean tumor uptake was determined to be 4.40 ± 0.29, 3.28 ± 0.47, and 2.04 ± 0.34 percentage of injected dose per gram of tissue (%ID/g) for ^{68}Ga−NOTA−Aca−BBN$_{7-14}$, and 2.99 ± 0.44, 2.96 ± 0.45, and 3.01 ± 0.45% ID/g for ^{68}Ga−NOTA−PEG$_3$−RM26 at 15, 30, and 60 min, with the corresponding P values of <0.01, 0.39, and 0.02, respectively, when comparing tumor uptake of the two tracers at the same time points post-injection.

However, the maximum tumor uptake was determined to be 6.68 ± 0.69, 5.14 ± 1.15, and 4.77 ± 0.96%ID/g for ^{68}Ga−NOTA−Aca−BBN$_{7-14}$, and 4.96 ± 0.87, 4.79 ± 0.98, and 4.91 ± 1.00%ID/g for ^{68}Ga−NOTA−PEG$_3$−RM26 at 15, 30, and 60 min, with the corresponding P values of 0.03, 0.68, and 0.85, respectively, when comparing the tumor uptake of the two tracers at the same time points post-injection.

Biodistribution of ^{68}Ga−NOTA−Aca−BBN$_{7-14}$ and ^{68}Ga−NOTA−PEG$_3$−RM26. The biodistribution of ^{68}Ga−NOTA−Aca−BBN$_{7-14}$ (n = 4) and ^{68}Ga−NOTA−PEG$_3$−RM26 (n = 3) in tumor and normal tissues determined by γ-counting was presented in Figure 6A. In good agreement with the PET images, high uptake and long retention of the radioactivity were observed for the GRPR-positive tissues including pancreas, intestine, and PC-3 tumor at 60 min post-injection, which were 17.99 ± 1.48, 4.33 ± 1.90, and 2.40 ± 0.38 ID/g for ^{68}Ga−NOTA−Aca−BBN$_{7-14}$ and 9.51 ± 0.73, 0.93 ± 0.12, and 3.31 ± 0.68%ID/g for ^{68}Ga−NOTA−PEG$_3$−RM26.

However, the tumor-to-lung, tumor-to-liver, tumor-to-kidney, tumor-to-pancreas, tumor-to-intestine, and tumor-to-muscle ratios for the radiopharmaceuticals at 1 h post-injection were shown in Figure 6B, which were 2.66, 9.66, 3.22, 0.34, 3.69, and 72.5 for ^{68}Ga−NOTA−PEG$_3$−RM26 and 5.34, 3.15, 1.52, 0.13. 0.56, and 25.57 for ^{68}Ga−NOTA−Aca−BBN$_{7-14}$, respectively. Except for the tumor-to-lung uptake ratios, ^{68}Ga−NOTA−PEG$_3$−RM26 showed much better tumor-to-organ contrast than that of ^{68}Ga−NOTA−Aca−BBN$_{7-14}$ (P values of <0.01 and <0.05). Specially, the tumor-to-muscle ratio of

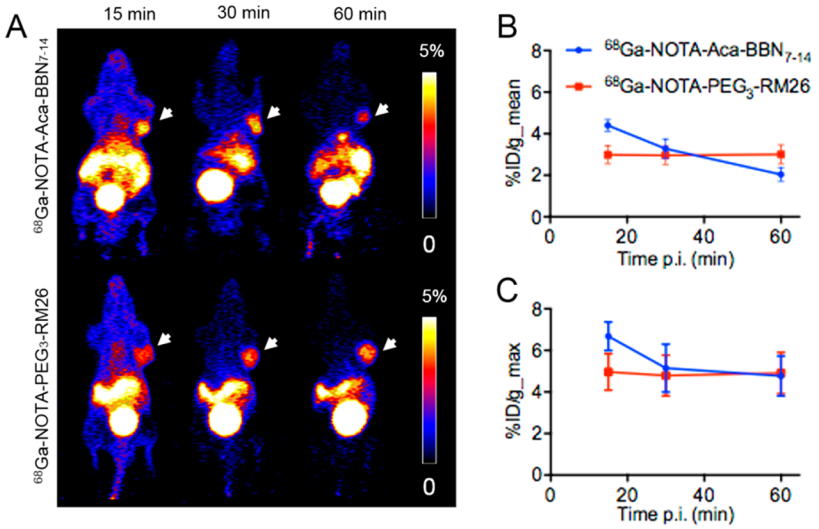

Figure 5. GRPR-specific imaging in PC-3 xenografted mouse model using ^{68}Ga−NOTA−Aca−BBN$_{7-14}$ and ^{68}Ga−NOTA−PEG$_3$−RM26. (A) Representative microcoronal PET scans of mice bearing PC-3 xenografts 15, 30, and 60 min after injection of ^{68}Ga−NOTA−Aca−BBN$_{7-14}$ and ^{68}Ga−NOTA−PEG$_3$−RM26. (B) PET quantification of tumor uptake in PC-3 tumors 15, 30, and 60 min after injection of ^{68}Ga−NOTA−Aca−BBN$_{7-14}$ (n = 4, mean ± SD) and ^{68}Ga−NOTA−PEG$_3$−RM26 (n = 3, mean ± SD), expressed as %ID/g_mean. (C) PET quantification of tumor uptake in PC-3 tumors 15, 30, and 60 min after the injection of ^{68}Ga−NOTA−Aca−BBN$_{7-14}$ (n = 4, mean ± SD) and ^{68}Ga−NOTA−PEG$_3$−RM26 (n = 3, mean ± SD), expressed as %ID/g_max.

DOI: 10.1021/acs.bioconjchem.7b00726
Bioconjugate Chem. 2018, 29, 410−419

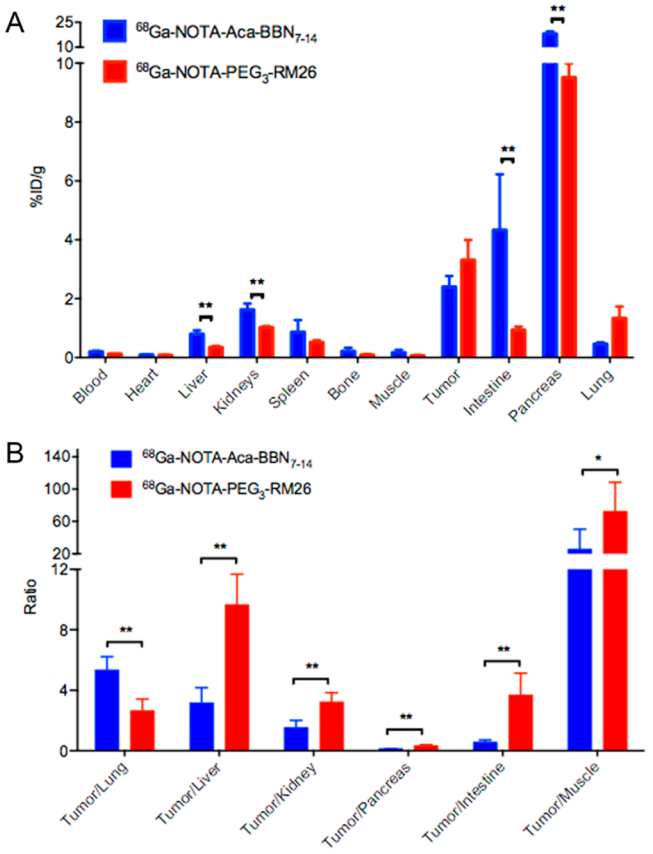

Figure 6. Biodistribution of ^{68}Ga−NOTA−Aca−BBN$_{7-14}$ (blue bars, n = 4) and ^{68}Ga−NOTA−PEG$_3$−RM26 (red bars, n = 3) in PC-3 tumor bearing nude mice at 60 min after administration (mean ± SD). (A) Biodistribution of ^{68}Ga−NOTA−Aca−BBN$_{7-14}$ and ^{68}Ga−NOTA−PEG$_3$−RM26 in multiple organs of PC-3 tumor bearing nude mice. Significant differences (P < 0.05) in biodistribution between probes were marked with asterisks. (B) Comparative ratios of the tumor uptake to major organs for ^{68}Ga−NOTA−Aca−BBN$_{7-14}$ and ^{68}Ga−NOTA−PEG$_3$−RM26 at 1 h post-injection. Significant differences (P values of <0.01 and <0.05) in tumor-to-organ ratios between probes were marked with asterisks.

^{68}Ga−NOTA−PEG$_3$−RM26 was 2.88-fold of that of the radio-agonist.

In Vivo Stability of ^{68}Ga−NOTA−Aca−BBN$_{7-14}$ and ^{68}Ga−NOTA−PEG$_3$−RM26. The in vivo metabolic stabilities of the radio conjugates were determined in each sample of mouse serum at 5 min after injection and in urine and tumor homogenates at 30 min after injection (Figure 7). The average extraction efficiencies were 89.3%, 97%, and 84.2% for serum, urine, and tumor, respectively. The composition of the metabolites was not identified, and almost all of the metabolites came earlier off the HPLC column than the parent compound for ^{68}Ga−NOTA−Aca−BBN$_{7-14}$, but the ^{68}Ga-NOTA-PEG$_3$-RM26 profile revealed a radio-metabolite with slightly higher lipophilicity that came off of the column after the parent compound. At 5 min post-injection, almost no parent form of ^{68}Ga−NOTA−Aca−BBN$_{7-14}$ was found in serum (Figure 7A); however, 88.92% of ^{68}Ga−NOTA−PEG$_3$−RM26 remained intact at the same time point (Figure 7B). In tumor, about 28.53% for ^{68}Ga−NOTA−Aca−BBN$_{7-14}$ (Figure 7C) and 79.74% for ^{68}Ga−NOTA−PEG$_3$−RM26 (Figure 7D) were intact. In urine, no parent form of either probe was observed (Figure 7E,F).

DISCUSSION

BBN analogues have been widely labeled with radionuclides such as ^{68}Ga, ^{64}Cu, ^{18}F, and ^{177}Lu.[8,20,22,23,37] In particular, ^{68}Ga can be easily produced due to the availability and commercialization of the in-house ^{68}Ge and ^{68}Ga generators (^{68}Ge, $t_{1/2}$ = 270.8 days). The ^{68}Ga-labeling of BBN derivatives conjugates come with high labeling yield, satisfactory radiochemical purity, and specific activity, and the clinical implementation of ^{68}Ga radiopharmaceuticals is preferred in the routine clinical setup of nuclear medicine. In this study, both BBN-based probes were prepared with high radiochemical purity and specific activity within 20 min, demonstrating ideal radiochemical processing for clinical translation.

In this study, we synthesized the NOTA-conjugated GRPR agonist BBN$_{7-14}$ and antagonist RM26; PEG$_3$ was used as a linker to conjugate NOTA to the antagonist peptide. The IC$_{50}$ values of NOTA−Aca−BBN$_{7-14}$ and NOTA−PEG$_3$−RM26 were similar to each other and also close to analogs reported from other laboratories previously.[31,33] Despite similar binding affinities, the tumor uptake of ^{68}Ga−NOTA−Aca−BBN$_{7-14}$ dropped rapidly from 4.40%ID/g at 15 min to 2.04%ID/g at 60 min post-injection in our study, and that of ^{68}Ga−NOTA−PEG$_3$−RM26 remained at a plateau of around 3.00%ID/g. The declining pattern of tumor uptake for ^{64}Cu-NOTA−Aca−BBN$_{7-14}$ in PC-3 tumor mice from 1 to 24 h post-injection has also been reported previously, and the authors speculate that the signal decrease was primarily due to rapid clearance from the bloodstream and excretion via the renal-urinary pathway.[22] Both ^{68}Ga−NOTA−Aca−BBN$_{7-14}$ and ^{68}Ga−NOTA−PEG$_3$−RM26 were mainly excreted through the urinary tract, so high accumulation of radioactivity in the bladder was observed. However, the kidney uptake was moderate compared with other peptide-based tracers.[38] Consistently, we observed most of ^{68}Ga−NOTA−PEG$_3$−RM26 in mouse serum remained intact at 5 min after injection, in comparison to 3.16% of ^{68}Ga−NOTA−Aca−BBN$_{7-14}$, indicating much greater metabolic stability in vivo for the antagonist and better suitability for GRPR imaging of ^{68}Ga−NOTA−PEG$_3$−RM26.

In agreement with the PET imaging study, the ex vivo biodistribution results further validated higher tumor-to-organ ratios for ^{68}Ga−NOTA−PEG$_3$−RM26 in comparison with those of ^{68}Ga−NOTA−Aca−BBN$_{7-14}$ at 60 min after injection. Hence, the higher tumor uptake and lower background offer ^{68}Ga−NOTA−PEG$_3$−RM26 more sensitivity in detecting indistinct lesions, such as metastasis distributed in the abdominal area in clinical settings.

It is well-known that introduction of different linkers between the metal chelator and targeting peptide sequence results in different tumor uptake and distinct normal organ distribution.[39,40] Indeed, we have included ^{68}Ga−NOTA−PEG$_3$−Aca-BBN$_{7-14}$ in the experimental design for this comparison study. However, both PET imaging and biodistribution results revealed that ^{68}Ga−NOTA−PEG$_3$−Aca-BBN$_{7-14}$ was the worst probe compared with the other two probes. The results indicated that the PEG$_3$ modification itself did not substantially alter the in vivo pharmacokinetics of BBN$_{7-14}$, and the difference between ^{68}Ga−NOTA−Aca−BBN$_{7-14}$ and ^{68}Ga−NOTA−PEG$_3$−RM26 mainly came from the inherent distinction of the peptide sequences and the agonism and antagonism of the two probes.

For in vitro stability assay, a minor portion of relatively hydrophilic radio peak was observed for ^{68}Ga−NOTA−Aca−

DOI: 10.1021/acs.bioconjchem.7b00726
Bioconjugate Chem. 2018, 29, 410−419

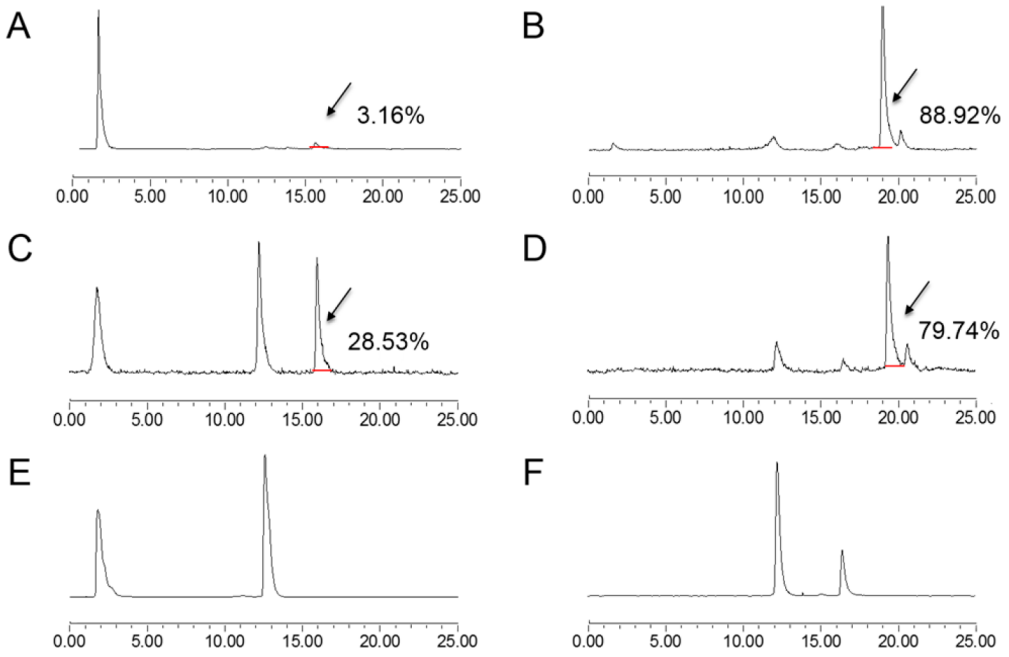

Figure 7. In vivo metabolic stabilities of ^{68}Ga−NOTA−Aca−BBN$_{7-14}$ and ^{68}Ga−NOTA−PEG$_3$−RM26, respectively, in serum at 5 min after injection and urine and tumor at 30 min after injection. (A) Stability of ^{68}Ga−NOTA−Aca−BBN$_{7-14}$ in serum at 5 min post-injection. (B) Stability of ^{68}Ga−NOTA−PEG$_3$−RM26 in serum at 5 min post-injection. (C) Stability of ^{68}Ga−NOTA−Aca−BBN$_{7-14}$ in tumor at 30 min post-injection. (D) Stability of ^{68}Ga−NOTA−PEG$_3$−RM26 in tumor at 30 min post-injection. (E) Stability of ^{68}Ga−NOTA−Aca−BBN$_{7-14}$ in urine at 30 min post-injection. (F) Stability of ^{68}Ga−NOTA−PEG$_3$−RM26 in urine at 30 min post-injection.

BBN$_{7-14}$ incubated in saline, which could result from radiolysis of the Met residue of ^{68}Ga−NOTA−Aca−BBN$_{7-14}$, while in FBS incubation, this kind of decomposition was possibly suppressed by the presence of serum proteins.[41,42] Moreover, a slightly more lipophilic radio peak was observed after 120 min incubation in nonheat inactivated FBS for both ^{68}Ga−NOTA−Aca−BBN$_{7-14}$ and ^{68}Ga−NOTA−PEG$_3$−RM26, each consisting 10.76% and 19.42% of the radiopharmaceuticals. Formation of these metabolites may have been derived from the action of serum proteases in nonheat inactivated FBS such as carboxamidase, which could catalyze the hydrolysis of C-terminal carboxamides to the corresponding carboxy acid.[43]

In vivo stability assay via radio-HPLC also indicated better stability of ^{68}Ga−NOTA−PEG$_3$−RM26 compared to ^{68}Ga−NOTA−Aca−BBN$_{7-14}$ in tumor homogenates. However, the structure of the radioactive fragments was not identified because the mass amount for the injection was limited. In a previous study, we observed a rapid degradation of BBN$_{7-14}$ during incubation in rat hepatocytes ($t_{1/2}$ = 4 min), and the metabolites of BBN$_{7-14}$ were found to be derived from peptide bond hydrolysis between amino acids Trp and Ala and between Ala and Val and within the C-terminal amide by high-resolution mass spectrometry coupled with HPLC (LC−MS).[44] Nevertheless, in vitro study does not necessarily represent the situation encountered by intravenously administered radiopeptides in vivo. Indeed, using in vivo mouse plasma metabolized fragment of ^{177}Lu−AMBA, the weak sites were revealed within the backbone of BBN$_{7-14}$ between amino acids Gln and Trp, Trp and Ala, and His and Leu, as well as the terminal amide of ^{177}Lu−AMBA.[43] It has been proposed and confirmed that neutral endopeptidase (NEP) acts as the major protease in the degradation of bombesin-like radiopeptides in vivo and that the co-injection of NEP inhibitors could enhance stability and tumor uptake of those radiopeptides.[45−47]

It is worth pointing out that a lack of stability is not an inherent issue for all GRPR agonists. Through structural interventions including peptide chain-length modification, amino acid substitutions, application of an amide-to-triazole replacement strategy, or the introduction of different lengths of spacer bridging the chelator to the peptide receptor-recognition site, the biological profiles (especially of radioligand pharmacokinetics in vivo) could be significantly improved.[45,48−50] The major hindrance of GRPR agonists is the possible biological effect induced upon receptor binding when a large amount of the agonists is administered for therapeutic purpose. A more-stable GRPR agonist may be still meaningful as an imaging probe.

CONCLUSIONS

The antagonist-based probe ^{68}Ga−NOTA−PEG$_3$−RM26 showed higher tumor uptake with lower background in the PC-3 tumor bearing mouse model at 1 h post-injection and displayed more-favorable in vivo pharmacokinetic properties as well as metabolic stabilities. ^{68}Ga−NOTA−PEG$_3$−RM26 is, therefore, a more-promising candidate for clinical translation of PET imaging for PCa compared to the agonist ^{68}Ga−NOTA−Aca−BBN$_{7-14}$.

MATERIALS AND METHODS

Chemistry. Aminocaproic acid (Aca)−BBN$_{7-14}$ and RM26 were synthesized using solid-phase Fmoc chemistry by Peptides International Inc. and CSBio. 1,4,7-Triazacyclononane-1,4,7-triacetic acid *N*-hydroxysuccinimide (NOTA−NHS) ester was purchased from CheMatech (Dijon, France). All other chemicals were obtained from Sigma-Aldrich. NOTA−Aca−BBN$_{7-14}$ and NOTA−PEG$_3$−RM26 were prepared according to a procedure published previously.[37]

DOI: 10.1021/acs.bioconjchem.7b00726
Bioconjugate Chem. 2018, 29, 410−419

^{68}Ga was eluted from a ^{68}Ge and ^{68}Ga generator (ITG) with 0.6 M HCl at 0.5 mL per fraction. A total of 0.5 mL of 1 M HEPES buffer was added to the fraction containing the most amount of ^{68}Ga radioactivity (185−222 MBq) to a final pH of around 6.0. A total of 10 μg of NOTA−Aca−BBN_{7-14} or NOTA−PEG_3−RM26 in 10 μL of water was added to the above solution. After shaking, the mixture was incubated at 80 °C for 10 min. The reaction mixture was trapped on an activated Varian Bond Elut C18 column (100 mg) by a syringe. Another 10 mL of water was used to wash the column, followed by 0.3 mL of 1 mM HCl ethanol solution to elute off the trapped radioactivity. Next, the product was diluted with saline for further use. An analytical reverse-phase radio HPLC (Waters Symmetry C-18 column, 3.9 × 150 mm, 5 μm) running a linear gradient starting from 5% A (0.1% TFA in acetonitrile) and 95% B (0.1% TFA in water) for 5 min and A increased to 65% at 2% per min, with the flow rate of 1 mL/min used for characterization of both tracers and in vitro and in vivo stability analysis.

In Vitro stability Test. The in vitro stability of ^{68}Ga−NOTA−Aca−BBN_{7-14} and ^{68}Ga−NOTA−PEG_3−RM26 was examined by radio HPLC according to a procedure reported previously.[51] Briefly, about 37 kilobecquerel (KBq) of ^{68}Ga−NOTA−Aca−BBN_{7-14} (40.0 MBq/nmol) or ^{68}Ga−NOTA−PEG_3−RM26 (39.8 MBq/nmol) in 50 μL was incubated in 450 μL of normal saline or FBS at 37 °C. At 0 and 120 min incubation, 25 μL of the saline-incubated sample was taken out of the tube and subjected to HPLC analysis. However, 25 μL of the serum sample was taken out at the same time points, added to an equal volume of acetonitrile, and centrifuged at 6000 rpm for 10 min. The supernatant was then extracted and submitted for radio-HPLC analysis.

Cell Culture and Animal Models. The PC-3 human prostate carcinoma cells were purchased from the American Type Culture Collection (ATCC, Rockville, MD). The cells were grown in Roswell Park Memorial Institute (RPMI) 1640 Medium supplemented with 10% FBS, penicillin (100 IU/mL), and streptomycin (100 mg/mL) (Invitrogen, Carlsbad, CA) and cultured at 37 °C in a humidified atmosphere containing 5% CO_2. Cells were passaged three times per week.

All animal studies were conducted according to the principles and procedures outlined in the Guide for the Care and Use of Laboratory Animals and were approved by the Institutional Animal Care and Use Committee of the Clinical Center, National Institutes of Health (NIH). Female BALB/c mice (age, 5−7 weeks; weights of 18−20 g) and female athymic nude/nude mice (age, 5−7 weeks; weights of 18−20 g) were purchased from Harlan Laboratories.

The PC-3 tumor models were generated by subcutaneous injection of 5 × 10^6 cells into the right shoulder of nude mice. Tumor sizes were measured using a digital caliper. Tumor volume (mm^3) was calculated according to the formula 0.5 × length × $width^2$. The mice were subjected to micro PET studies when the tumor volume reached 100−300 mm^3 (3−4 weeks after inoculation).

In Vitro Cell Receptor Binding Assay. In vitro GRPR-binding affinities and specificities of BBN_{7-14}, PEG_3-RM26, NOTA−Aca−BBN_{7-14}, and NOTA−PEG_3−RM26 were determined by displacement PC-3 cell-binding assays using ^{125}I−[Tyr4]BBN as the radioligand. ^{125}I−[Tyr4]BBN (81 400 gigabecquerel (GBq)/mmol) was purchased from American Radiolabeled Chemicals, Inc. Experiments were performed on PC-3 cells by modifying a previously described method.[52] Briefly, PC-3 cells were freshly harvested and seeded in 96-well plates at 10^5 cells/50 μL per well in RMPI 1640 binding buffer (with 0.1% bovine serum albumin, serum free). ^{125}I−Tyr4]BBN was diluted in binding buffer with a specific activity of 2.2 KBq/50 μL. The cells and diluted ^{125}I−[Tyr4]BBN were then incubated, respectively, with increasing concentrations of BBN_{7-14}, PEG_3-RM26, NOTA−Aca−BBN_{7-14}, and NOTA−PEG_3−RM26 ranging from 0 to 2000 nmol/L in 37 °C up to 60 min. The IC_{50} values were determined by nonlinear regression analysis using Graph-Pad Prism (GraphPad Software, Inc.). Experiments were performed in triplicate.

Cell Uptake and Internalization Studies. The uptake and internalization of ^{68}Ga−NOTA−Aca−BBN_{7-14} and ^{68}Ga−NOTA−PEG_3−RM26 in PC-3 cells were examined according to the following procedures, respectively. For the cell uptake experiment, PC-3 cells were seeded in 24-well plates at a density of 10^5 cells per well 24 h before the assay. The medium was removed, and the cells were rinsed twice with PBS. Then, 7.4 KBq per well of tracers (with the corresponding specific activities of 40.0 MBq/nmol and 53.3 MBq/nmol for ^{68}Ga−NOTA−Aca−BBN_{7-14} and ^{68}Ga−NOTA−PEG_3−RM26) were added in 0.5 mL of serum-free media (SFM). The cells were incubated at 37 °C for 5, 15, 30, and 60 min. At each indicated time point, the medium was removed, and cells were rinsed twice with cold PBS (1 mL) and lysed by the addition of 0.2 mL of 0.1 M NaOH. The cell lysate was collected for γ-counting. For internalization study, after the removal of the medium at the same indicated time point as the cell uptake study, the cells were incubated for 1 min with 0.5 mL of acid buffer (50 mM glycine and 100 mM NaCl at pH 2.8). Next, the acid buffer was removed, and the cells were washed twice with 1 mL of PBS, followed by addition of 0.2 mL of 0.1 M NaOH. Cell lysate was collected, and the radioactivity was measured by a γ-counter. The cell uptake and internalization values were normalized to the amount of added radioactivity. Each experiment was performed in triplicate.

Cell Efflux Studies. For a cell-efflux study of ^{68}Ga−NOTA−Aca−BBN_{7-14} (39.8 MBq/nmol)and ^{68}Ga−NOTA−PEG_3−RM26 (52.5 MBq/nmol), 7.4 KBq per well of tracers were added to PC-3 cells in a 24-well plate and incubated for 1 h at 37 °C. Next, cells were washed twice with cold PBS and incubated with SFM for 5, 15, 30, and 60 min. After being washed twice with PBS, cells were harvested by the addition of 0.2 mL of 0.1 mol/L NaOH. Cell lysate was collected and the radioactivity measured by a γ-counter. Efflux values were calculated by subtracting retention at different time points from 0 min retention and normalized by dividing the total counts at 0 min.

PET of Tumor-Bearing Mice. PET scans were obtained using an Inveon small animal PET scanner (Siemens Medical Solutions). Under isoflurane anesthesia, 5 min of static PET scanning was performed at 15, 30, and 60 min after the PC-3 tumor-bearing mice were each intravenously injected with 3.7 MBq of ^{68}Ga−NOTA−Aca−BBN_{7-14} (28.2 MBq/nmol) (n = 4) or ^{68}Ga−NOTA−PEG_3−RM26 (32.6 MBq/nmol) (n = 3) in a volume of 100 μL of PBS.

The PET images were reconstructed using 3-dimensional ordered-subsets expectation maximum (3D OSEM) followed by maximum a posteriori (MAP) algorithm with a smoothing parameter (OSEM-3D-MAP) of 0.1. For each scan, regions of interest (ROIs) were drawn over the tumor on whole-body decay-corrected coronal images using vendor software (ASI Pro 5.2.4.0; Siemens Medical Solutions). The radioactivity accu-

DOI: 10.1021/acs.bioconjchem.7b00726
Bioconjugate Chem. 2018, 29, 410−419

mulation within the tumor was calculated from mean pixel values of the multiple ROI volumes. These values were converted to MBq/mL and then further divided by the administered activity to obtain an image-ROI-derived %ID/g value (assuming a tissue density of 1 g/mL). No correction was applied in this study.

Biodistribution of ^{68}Ga−NOTA−Aca−BBN$_{7-14}$ and ^{68}Ga−NOTA−PEG$_3$−RM26. Each mouse was intravenously injected with 3.7 MBq of ^{68}Ga−NOTA−Aca−BBN$_{7-14}$ (28.2 MBq/nmol) (n = 4) or ^{68}Ga−NOTA−PEG$_3$−RM26 (32.6 MBq/nmol) (n = 3) in a volume of 100 μL of PBS. At 1 h post-injection, the mice were sacrificed, and blood, heart, liver, kidneys, spleen, bone, muscle, tumor, intestine, pancreas, and lung tissues were collected. The organs were wet-weighed, and the radioactivity was assayed using a γ-counter.

In Vivo Stability of ^{68}Ga−NOTA−Aca−BBN$_{7-14}$ and ^{68}Ga−NOTA−PEG3−RM26. For serum metabolic stability studies, each healthy Balb/c mouse was injected intravenously with 37 MBq of ^{68}Ga−NOTA−Aca−BBN$_{7-14}$ (34.9 MBq/nmol) or ^{68}Ga−NOTA−PEG$_3$−RM26 (46.8 MBq/nmol). At 5 min after injection, the mice were anesthetized, and 100 μL of blood was collected. The blood sample was immediately centrifuged at 13 200 rpm for 5 min. A total of 25 μL of the supernatant was removed and mixed with an equal volume of acetonitrile, with centrifugation at 6000 rpm for 10 min. Next, the extracted solution was injected into an HPLC device for analysis. For urine analysis, the urine was collected at 30 min post-injection, and then 25 μL of the urine was mixed with an equal volume of acetonitrile and centrifuged at 13 200 rpm for 5 min. The supernatant was moved and subjected to HPLC analysis.

For tumor metabolism analysis, a pair of PC-3 tumor bearing mice were injected with 37 MBq of each tracer (with the specific activities of 32.9 and 31.6 MBq/nmol for of ^{68}Ga−NOTA−Aca−BBN$_{7-14}$ and ^{68}Ga−NOTA−PEG$_3$−RM26, respectively). At 30 min after injection, the mice were sacrificed under anesthesia, and the tumors were removed and weighed. With an equal weight of acetonitrile, the tumor was homogenized on ice and centrifuged at 13 200 rpm for 5 min. A total of 50 μL of the supernatant was removed for HPLC analysis.

The radioactivity of in vivo collected blood, urine, and tumor samples was measured with a γ-counter each time before and after the samples were homogenized or centrifuged to calculate the extraction efficiency. All samples were collected in pre-chilled vials, and all further manipulations were conducted on ice or at 4 °C for centrifugation to prevent further degradation during sample workup.

Statistical Analysis. All quantitative data are presented as mean ± SD. Mean values were compared using one-way ANOVA and the Student t test. P values of <0.05 were considered statistically significant.

AUTHOR INFORMATION

Corresponding Authors

*E-mail: evazhu@vip.sina.com.
*E-mail: niug@mail.nih.gov.
*E-mail: shawn.chen@nih.gov.

ORCID

Xiaoyuan Chen: 0000-0002-9622-0870

Notes

The authors declare no competing financial interest.

ACKNOWLEDGMENTS

This work was supported by the National Natural Science Foundation of China (grant nos. 81671718 and 81271600), Natural Science Foundation of Hubei Province of China (grant no. 2016CFB687), and the Intramural Research Program of the National Institute of Biomedical Imaging and Bioengineering, National Institutes of Health. S.C. is a Ph.D. candidate of Tongji Medical College, Huazhong University of Science and Technology, and is partially funded by the China Scholarship Council (CSC) as a visiting student of NIH.

REFERENCES

(1) Siegel, R. L., Miller, K. D., and Jemal, A. (2017) Cancer Statistics, 2017. *Ca-Cancer J. Clin. 67*, 7−30.

(2) Mottet, N., Bellmunt, J., Bolla, M., Briers, E., Cumberbatch, M. G., De Santis, M., Fossati, N., Gross, T., Henry, A. M., Joniau, S., et al. (2017) EAU-ESTRO-SIOG Guidelines on Prostate Cancer. Part 1: Screening, Diagnosis, and Local Treatment with Curative Intent. *Eur. Urol. 71*, 618−629.

(3) Schuster, D. M., Nanni, C., and Fanti, S. (2016) PET Tracers Beyond FDG in Prostate Cancer. *Semin. Nucl. Med. 46*, 507−521.

(4) Barentsz, J. O., Richenberg, J., Clements, R., Choyke, P., Verma, S., Villeirs, G., Rouviere, O., Logager, V., and Futterer, J. J. (2012) ESUR prostate MR guidelines 2012. *Eur. Radiol. 22*, 746−757.

(5) Verma, S., Rajesh, A., Futterer, J. J., Turkbey, B., Scheenen, T. W., Pang, Y., Choyke, P. L., and Kurhanewicz, J. (2010) Prostate MRI and 3D MR Spectroscopy: How We Do It. *AJR, Am. J. Roentgenol. 194*, 1414−1426.

(6) Murphy, G., Haider, M., Ghai, S., and Sreeharsha, B. (2013) The Expanding Role of MRI in Prostate Cancer. *AJR, Am. J. Roentgenol. 201*, 1229−1238.

(7) Woo, S., Suh, C. H., Kim, S. Y., Cho, J. Y., and Kim, S. H. (2017) Diagnostic Performance of Prostate Imaging Reporting and Data System Version 2 for Detection of Prostate Cancer: A Systematic Review and Diagnostic Meta-analysis. *Eur. Urol. 72*, 177−188.

(8) Schoder, H., Herrmann, K., Gonen, M., Hricak, H., Eberhard, S., Scardino, P., Scher, H. I., and Larson, S. M. (2005) 2-[^{18}F]Fluoro-2-deoxyglucose Positron Emission Tomography for the Detection of Disease in Patients with Prostate-Specific Antigen Relapse After Radical Prostatectomy. *Clin. Cancer Res. 11*, 4761−4769.

(9) Wibmer, A. G., Burger, I. A., Sala, E., Hricak, H., Weber, W. A., and Vargas, H. A. (2016) Molecular Imaging of Prostate Cancer. *Radiographics 36*, 142−159.

(10) Schuster, D. M., Nanni, C., and Fanti, S. (2016) Evaluation of Prostate Cancer with Radiolabeled Amino Acid Analogs. *J. Nucl. Med. 57*, 61S−66S.

(11) Jadvar, H. (2011) Prostate Cancer: PET with ^{18}F-FDG, ^{18}F- or ^{11}C-acetate, and ^{18}F- or ^{11}C-choline. *J. Nucl. Med. 52*, 81−89.

(12) Schwarzenbock, S. M., Rauscher, I., Bluemel, C., Fendler, W. P., Rowe, S. P., Pomper, M. G., Asfhar-Oromieh, A., Herrmann, K., and Eiber, M. (2017) PSMA Ligands for PET-Imaging of Prostate Cancer. *J. Nucl. Med. 58*, 1545−1552.

(13) Ceci, F., Herrmann, K., Hadaschik, B., Castellucci, P., and Fanti, S. (2017) Therapy Assessment in Prostate Cancer Using Choline and PSMA PET/CT. *Eur. J. Nucl. Med. Mol. Imaging 44* (1), 78−83.

(14) Bach-Gansmo, T., Nanni, C., Nieh, P. T., Zanoni, L., Bogsrud, T. V., Sletten, H., Korsan, K. A., Kieboom, J., Tade, F. I., Odewole, O., et al. (2017) Multisite Experience of the Safety, Detection Rate and Diagnostic Performance of Fluciclovine (^{18}F) Positron Emission Tomography/Computerized Tomography Imaging in the Staging of Biochemically Recurrent Prostate Cancer. *J. Urol. 197*, 676−683.

(15) Guo, M., Qu, X., and Qin, X. Q. (2015) Bombesin-Like Peptides and Their Receptors: Recent Findings in Pharmacology and Physiology. *Curr. Opin. Endocrinol., Diabetes Obes. 22*, 3−8.

(16) Patel, O., Shulkes, A., and Baldwin, G. S. (2006) Gastrin-Releasing Peptide and Cancer. *Biochim. Biophys. Acta, Rev. Cancer 1766*, 23−41.

DOI: 10.1021/acs.bioconjchem.7b00726
Bioconjugate Chem. 2018, 29, 410−419

(17) Morgat, C., MacGrogan, G., Brouste, V., Velasco, V., Sevenet, N., Bonnefoi, H., Fernandez, P., Debled, M., and Hindie, E. (2017) Expression of Gastrin-Releasing Peptide Receptor (GRPR) in Breast Cancer and its Association with Pathologic, Biologic and Clinical Parameters: A Study of 1432 Primary Tumors. *J. Nucl. Med. 58*, 1401−1407.
(18) Sancho, V., Di Florio, A., Moody, T. W., and Jensen, R. T. (2011) Bombesin Receptor-Mediated Imaging and Cytotoxicity: Review and Current Status. *Curr. Drug Delivery 8*, 79−134.
(19) Ferreira, C. A., Fuscaldi, L. L., Townsend, D. M., Rubello, D., and Barros, A. L. B. (2017) Radiolabeled Bombesin Derivatives for Preclinical Oncological Imaging. *Biomed. Pharmacother. 87*, 58−72.
(20) Smith, C. J., Gali, H., Sieckman, G. L., Hayes, D. L., Owen, N. K., Mazuru, D. G., Volkert, W. A., and Hoffman, T. J. (2003) Radiochemical Investigations of ^{177}Lu-DOTA-8-Aoc-BBN[7−14]NH_2: An In Vitro/In Vivo Assessment of the Targeting Ability of This New Radiopharmaceutical for PC-3 Human Prostate Cancer Cells. *Nucl. Med. Biol. 30*, 101−109.
(21) Smith, C. J., Gali, H., Sieckman, G. L., Higginbotham, C., Volkert, W. A., and Hoffman, T. J. (2003) Radiochemical Investigations of ^{99m}Tc-N_3S-X-BBN[7−14]NH_2: An In Vitro/In Vivo Structure-Activity Relationship Study Where X = 0-, 3-, 5-, 8-, and 11-Carbon Tethering Moieties. *Bioconjugate Chem. 14*, 93−102.
(22) Prasanphanich, A. F., Nanda, P. K., Rold, T. L., Ma, L., Lewis, M. R., Garrison, J. C., Hoffman, T. J., Sieckman, G. L., Figueroa, S. D., and Smith, C. J. (2007) [^{64}Cu-NOTA-8-Aoc-BBN(7−14)NH_2] Targeting Vector for Positron-Emission Tomography Imaging of Gastrin-Releasing Peptide Receptor-Expressing Tissues. *Proc. Natl. Acad. Sci. U. S. A. 104*, 12462−12467.
(23) Zhang, J., Li, D., Lang, L., Zhu, Z., Wang, L., Wu, P., Niu, G., Li, F., and Chen, X. (2016) ^{68}Ga-NOTA−Aca−BBN(7−14) PET/CT in Healthy Volunteers and Glioma Patients. *J. Nucl. Med. 57*, 9−14.
(24) Minamimoto, R., Hancock, S., Schneider, B., Chin, F. T., Jamali, M., Loening, A., Vasanawala, S., Gambhir, S. S., and Iagaru, A. (2016) Pilot Comparison of ^{68}Ga-RM2 PET and ^{68}Ga-PSMA-11 PET in Patients with Biochemically Recurrent Prostate Cancer. *J. Nucl. Med. 57*, 557−562.
(25) Wieser, G., Popp, I., Christian Rischke, H., Drendel, V., Grosu, A. L., Bartholoma, M., Weber, W. A., Mansi, R., Wetterauer, U., Schultze-Seemann, W., et al. (2017) Diagnosis of Recurrent Prostate Cancer with PET/CT Imaging Using the Gastrin-Releasing Peptide Receptor Antagonist ^{68}Ga-RM2: Preliminary Results in Patients with Negative or Inconclusive [^{18}F]Fluoroethylcholine-PET/CT. *Eur. J. Nucl. Med. Mol. Imaging 44*, 1463−1472.
(26) Maina, T., Bergsma, H., Kulkarni, H. R., Mueller, D., Charalambidis, D., Krenning, E. P., Nock, B. A., de Jong, M., and Baum, R. P. (2016) Preclinical and first clinical experience with the gastrin-releasing peptide receptor-antagonist [^{68}Ga]SB3 and PET/CT. *Eur. J. Nucl. Med. Mol. Imaging 43*, 964−973.
(27) Kahkonen, E., Jambor, I., Kemppainen, J., Lehtio, K., Gronroos, T. J., Kuisma, A., Luoto, P., Sipila, H. J., Tolvanen, T., Alanen, K., et al. (2013) In Vivo Imaging of Prostate Cancer Using [^{68}Ga]-Labeled Bombesin Analog BAY86−7548. *Clin. Cancer Res. 19*, 5434−5443.
(28) Wieser, G., Mansi, R., Grosu, A. L., Schultze-Seemann, W., Dumont-Walter, R. A., Meyer, P. T., Maecke, H. R., Reubi, J. C., and Weber, W. A. (2014) Positron Emission Tomography (PET) Imaging of Prostate Cancer with a Gastrin Releasing Peptide Receptor Antagonist–From Mice to Men. *Theranostics 4*, 412−419.
(29) Llinares, M., Devin, C., Chaloin, O., Azay, J., Noel-Artis, A. M., Bernad, N., Fehrentz, J. A., and Martinez, J. (1999) Syntheses and Biological Activities of Potent Bombesin Receptor Antagonists. *J. Pept. Res. 53*, 275−283.
(30) Varasteh, Z., Velikyan, I., Lindeberg, G., Sorensen, J., Larhed, M., Sandstrom, M., Selvaraju, R. K., Malmberg, J., Tolmachev, V., and Orlova, A. (2013) Synthesis and Characterization of a High-Affinity NOTA-Conjugated Bombesin Antagonist for GRPR-Targeted Tumor Imaging. *Bioconjugate Chem. 24*, 1144−1153.
(31) Varasteh, Z., Mitran, B., Rosenstrom, U., Velikyan, I., Rosestedt, M., Lindeberg, G., Sorensen, J., Larhed, M., Tolmachev, V., and Orlova, A. (2015) The Effect of Macrocyclic Chelators on the Targeting Properties of the ^{68}Ga-Labeled Gastrin Releasing Peptide Receptor Antagonist PEG2-RM26. *Nucl. Med. Biol. 42*, 446−454.
(32) Mitran, B., Varasteh, Z., Selvaraju, R. K., Lindeberg, G., Sorensen, J., Larhed, M., Tolmachev, V., Rosenstrom, U., and Orlova, A. (2016) Selection of Optimal Chelator Improves the Contrast of GRPR Imaging Using Bombesin Analogue RM26. *Int. J. Oncol. 48*, 2124−2134.
(33) Ginj, M., Zhang, H., Waser, B., Cescato, R., Wild, D., Wang, X., Erchegyi, J., Rivier, J., Macke, H. R., and Reubi, J. C. (2006) Radiolabeled Somatostatin Receptor Antagonists Are Preferable to Agonists for In Vivo Peptide Receptor Targeting of Tumors. *Proc. Natl. Acad. Sci. U. S. A. 103*, 16436−16441.
(34) Cescato, R., Maina, T., Nock, B., Nikolopoulou, A., Charalambidis, D., Piccand, V., and Reubi, J. C. (2008) Bombesin Receptor Antagonists May Be Preferable to Agonists for Tumor Targeting. *J. Nucl. Med. 49*, 318−326.
(35) Yang, M., Gao, H., Zhou, Y., Ma, Y., Quan, Q., Lang, L., Chen, K., Niu, G., Yan, Y., and Chen, X. (2011) F-Labeled GRPR Agonists and Antagonists: A Comparative Study in Prostate Cancer Imaging. *Theranostics 1*, 220−229.
(36) Yu, Z., Ananias, H. J., Carlucci, G., Hoving, H. D., Helfrich, W., Dierckx, R. A., Wang, F., de Jong, I. J., and Elsinga, P. H. (2013) An Update of Radiolabeled Bombesin Analogs for Gastrin-Releasing Peptide Receptor Targeting. *Curr. Pharm. Des. 19*, 3329−3341.
(37) Liu, Z., Niu, G., Wang, F., and Chen, X. (2009) ^{68}Ga-Labeled NOTA-RGD-BBN Peptide for Dual Integrin and GRPR-Targeted Tumor Imaging. *Eur. J. Nucl. Med. Mol. Imaging 36*, 1483−1494.
(38) Lin, M., Welch, M. J., and Lapi, S. E. (2013) Effects of Chelator Modifications on ^{68}Ga-Labeled [Tyr^3]Octreotide Conjugates. *Mol. Imaging Biol. 15*, 606−613.
(39) Guo, H., Yang, J., Gallazzi, F., and Miao, Y. (2011) Effects of the Amino Acid Linkers on the Melanoma-Targeting and Pharmacokinetic Properties of ^{111}In-Labeled Lactam Bridge-Cyclized Alpha-MSH Peptides. *J. Nucl. Med. 52*, 608−616.
(40) Mansi, R., Wang, X., Forrer, F., Waser, B., Cescato, R., Graham, K., Borkowski, S., Reubi, J. C., and Maecke, H. R. (2011) Development of a Potent DOTA-Conjugated Bombesin Antagonist for Targeting GRPr-Positive Tumours. *Eur. J. Nucl. Med. Mol. Imaging 38*, 97−107.
(41) Chen, J., Linder, K. E., Cagnolini, A., Metcalfe, E., Raju, N., Tweedle, M. F., and Swenson, R. E. (2008) Synthesis, Stabilization and Formulation of [^{177}Lu]Lu-AMBA, a Systemic Radiotherapeutic Agent for Gastrin Releasing Peptide Receptor Positive Tumors. *Appl. Radiat. Isot. 66*, 497−505.
(42) Cagnolini, A., Chen, J., Ramos, K., Skedzielewski, T. M., Lantry, L. E., Nunn, A. D., Swenson, R. E., and Linder, K. E. (2010) Automated Synthesis, Characterization and Biological Evaluation of [^{68}Ga]Ga-AMBA, and the Synthesis and Characterization of ^{nat}Ga-AMBA and [^{67}Ga]Ga-AMBA. *Appl. Radiat. Isot. 68*, 2285−2292.
(43) Linder, K. E., Metcalfe, E., Arunachalam, T., Chen, J., Eaton, S. M., Feng, W., Fan, H., Raju, N., Cagnolini, A., Lantry, L. E., et al. (2009) In Vitro and In Vivo Metabolism of Lu-AMBA, a GRP-Receptor Binding Compound, and the Synthesis and Characterization of Its Metabolites. *Bioconjugate Chem. 20*, 1171−1178.
(44) Ma, Y., Yang, M., Gao, H., Niu, G., Yan, Y., Lang, L., Kiesewetter, D. O., and Chen, X. (2012) Evaluation of Fluorine-Labeled Gastrin-Releasing Peptide Receptor (GRPR) Agonists and Antagonists by LC/MS. *Amino Acids 43*, 1625−1632.
(45) Maina, T., Kaloudi, A., Valverde, I. E., Mindt, T. L., and Nock, B. A. (2017) Amide-to-Triazole Switch vs. In Vivo NEP-Inhibition Approaches to Promote Radiopeptide Targeting of GRPR-Positive Tumors. *Nucl. Med. Biol. 52*, 57−62.
(46) Nock, B. A., Maina, T., Krenning, E. P., and de Jong, M. (2014) "To Serve and Protect": Enzyme Inhibitors as Radiopeptide Escorts Promote Tumor Targeting. *J. Nucl. Med. 55*, 121−127.
(47) Shipp, M. A., Tarr, G. E., Chen, C. Y., Switzer, S. N., Hersh, L. B., Stein, H., Sunday, M. E., and Reinherz, E. L. (1991) CD10/Neutral Endopeptidase 24.11 Hydrolyzes Bombesin-Like Peptides and

DOI: 10.1021/acs.bioconjchem.7b00726
Bioconjugate Chem. 2018, 29, 410−419

Regulates the Growth of Small Cell Carcinomas of the Lung. *Proc. Natl. Acad. Sci. U. S. A. 88*, 10662−10666.
(48) Fani, M., and Maecke, H. R. (2012) Radiopharmaceutical Development of Radiolabelled Peptides. *Eur. J. Nucl. Med. Mol. Imaging 39* (1), 11−30.
(49) Mascarin, A., Valverde, I. E., Vomstein, S., and Mindt, T. L. (2015) 1,2,3-Triazole Stabilized Neurotensin-Based Radiopeptidomimetics for Improved Tumor Targeting. *Bioconjugate Chem. 26*, 2143−2152.
(50) Valverde, I. E., Vomstein, S., and Mindt, T. L. (2016) Toward the Optimization of Bombesin-Based Radiotracers for Tumor Targeting. *J. Med. Chem. 59*, 3867−3877.
(51) Lang, L., Ma, Y., Kiesewetter, D. O., and Chen, X. (2014) Stability Analysis of Glutamic Acid Linked Peptides Coupled to NOTA Through Different Chemical Linkages. *Mol. Pharmaceutics 11*, 3867−3874.
(52) Chen, X., Park, R., Hou, Y., Tohme, M., Shahinian, A. H., Bading, J. R., and Conti, P. S. (2004) MicroPET and Autoradiographic Imaging of GRP Receptor Expression with ^{64}Cu-DOTA-[Lys^{3}]-Bombesin in Human Prostate Adenocarcinoma Xenografts. *J. Nucl. Med. 45*, 1390−1397.

DOI: 10.1021/acs.bioconjchem.7b00726
Bioconjugate Chem. 2018, 29, 410−419